Analysis of Microwave Propagation Attenuation on Traveling-Wave Mach-Zehnder Modulators

Ruoyun Yao
College of Information Science and Electronic Engineering
Zhejiang University
Hangzhou, China
yaoruoyun@zju.edu.cn

Weiwei Pan
College of Information Science and Electronic Engineering
Zhejiang University
Hangzhou, China
weiweipan@zju.edu.cn

Yili Liu
Research Institute of Intelligent Networks
Zhejiang Lab
Hangzhou, China
liuyl@zhejianglab.com

Zhangwan Peng
College of Information Science and Electronic Engineering
Zhejiang University
Hangzhou, China
pengzhangwan@zju.edu.cn

Yiti Xiong
Research Institute of Intelligent Networks
Zhejiang Lab
Hangzhou, China
xiongyt@zju.edu.cn

Chen Ji
College of Information Science and Electronic Engineering
Zhejiang University
Hangzhou, China
chen.ji@zju.edu.cn

***Abstract*—We present in-depth analysis on multiple microwave loss mechanisms in the total attenuation of high-speed traveling-wave Mach-Zehnder modulators, including the p-type dopant induced transverse and longitudinal semiconductor losses by full-wave simulation.**

Keywords—high-speed, Mach-Zehnder modulator, microwave loss, p-type dopant, traveling-wave

I. Introduction

For the up-coming 800 G and 1.6 T datacom transmission technologies, high speed traveling-wave Mach-Zehnder modulator (MZM) on InP is the most likely solution delivering the necessary operating speed for beyond 200 Gb/s per lane PAM4 transmission [1]. The keys to achieve ultra-wide modulation bandwidth in the traveling-wave scheme are propagation speed matching between optical and electrical waves, impedance matching between the modulator and the external electrical system, and microwave attenuation associated with both traveling-wave electrode (TWE) structures and underlying semiconductor layers [2], [3]. Up till now, multiple solutions have been proposed and demonstrated to achieve simultaneously velocity and impedance matching with the assist of various equivalent circuit models for lossless transmission line by empirical calculations [4]. However, in most reported research, the microwave propagation attenuation factor has been tacitly ignored in TWE-MZM high-speed performance analysis, which implies a challenging and promising scenario in extending the optical transmission rate to 200 Gb/s and beyond [5]. The major source of microwave propagation attenuation in InP modulators can be attributed to the poor microwave property associated with the p-cladding layer. Recent progress of MZM mostly revolved around replacing the thick p-cladding layer with other materials contributing to low series resistance [6], which will inevitably lead to increased fabrication complexity and production cost for volume commercial applications correspondingly.

In this work, we present in-depth analysis of microwave propagation attenuation for a typical TWE-MZM with a general p-i-n type epitaxial structure, which is assumed to meet the velocity and impedance matching demands. Multiple loss mechanisms in the total attenuation of TWE-MZM, including the p-cladding layer induced transverse and longitudinal semiconductor losses, are investigated for the first time by full-wave simulation in commercial software (HFSS). Our simulation results demonstrate that in a light p-type doping regime, the transverse semiconductor loss dominants the microwave attenuation; while in a heavy p-type doping regime, the longitudinal semiconductor loss plays a leading role instead.

This work was supported in part by the National key research & development (R&D) plan 2020YFB1805701, and the Zhejiang Lab grant. 2020LC0AD01/001.

II. Device Modeling

A typical cross section of a capacitive loading TWE MZM with a 2.2 μm wide shallow-etched ridge stopping at the undoped upper spacer layer is illustrated in Fig. 1. The epitaxial structure of the MZM is grown on a semi-insulating (S.I.) InP substrate, including from bottom up a 1.7 μm InP n-mesa layer (1×10^{18} cm^{-3}), a 0.296 μm undoped lower InP spacer layer, a 0.408 μm undoped InGaAsP multi-quantum well (MQW) active region, a 0.396 μm undoped upper InP spacer layer, a 1.3 μm InP p-cladding layer (5×10^{17} cm^{-3}) and a 0.2 μm $In_{0.53}Ga_{0.47}As$ p-contact layer (1×10^{19} cm^{-3}). The corresponding material data is listed in Table I. For our case study, we use data for the InP/InGaAsP material system according to self-developing devices. However, the model as such is not restricted to this material system.

The network in Fig. 2 describes a unit length of a TWE section, with the conductor resistance for the metal electrode (R_c), series resistance for p-cladding layer (R_p) and n-cladding layer (R_n). We note that an additional resistance R_{sc}, which represents the loss arising from a longitudinal induced current in the semiconductor material, is also included [3]. The semiconductor loss corresponding to R_{sc} has been demonstrated to be proportional to ω^2 and typically dominates

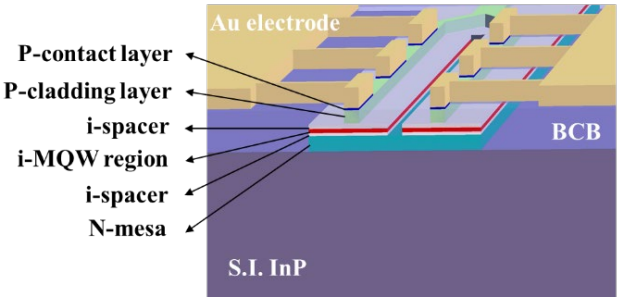

Fig. 1. A typical TWE-MZM structure. This figure inlustrates a capacitive loading TWE configuration. The optical waveguide is present with 2.2 μm wide shallow-etched ridges stopping at the undoped upper spacer layer.

TABLE I. ASSUMED MATERIAL DATA USED FOR SIMULATION [7]

Material	*Relative Permittivity*	*Conductivity (S/m)*
p-$In_{0.53}Ga_{0.47}As$ (1×10^{19} cm^{-3})	13.9	69183
p-InP (5×10^{17} cm^{-3})	12.56	1201
i-InP	12.56	-
i-InGaAsP	13.21	-
n-InP (1×10^{18} cm^{-3})	12.56	41120
S.I. InP	12.56	-
BCB	2.6	-
gold	1	4.1×10^{7}

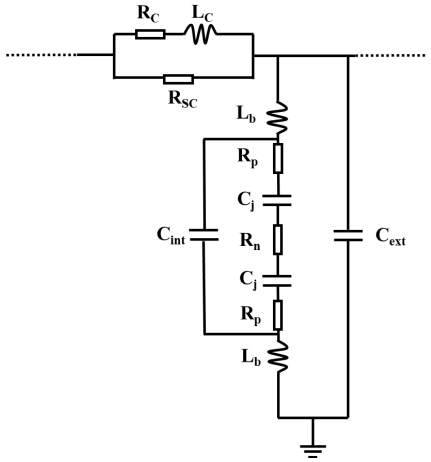

Fig. 2. Equivalent circuit for a unit length of the TWE.

at high frequencies, whereas the metal loss (R_c) dominates at low frequencies [8]. L_c and L_b are the self-inductances of the CPS electrode and the connecting bridge between external and internal metal electrode structures. The total capacitance per unit length is obtained as the superposition of the capacitances of the internal electrode (C_{int}), external electrode (C_{ext}) and back-to-back serially connected depletion layers ($C_j/2$).

In previous analysis, the capacitance value is optimized to meet the simultaneously velocity and impedance matching demands but the microwave propagation attenuation from semiconductor resistance is tacitly ignored [4], [5]. Actually, microwave propagation attenuation from transverse semiconductor loss (R_p) and longitudinal semiconductor loss (R_{sc}) are significant in TWE design, especially at high frequencies [8], presenting a bottleneck in modulation bandwidth of InP MZM. The mentioned two semiconductor RF loss contributions are both highly sensitive to p-cladding layer doping profile due to its poor conductivity, i.e., the conductivity of the p-cladding layer affects both R_p and R_{sc}. In light doping regimes, the conductivity of the p-cladding layer is lower than in heavy doping regimes. Hence, we infer that there exists an optimum value for the p-doping concentration, leading to minimized microwave attenuation.

III. DISCUSSIN

We explicitly calculated microwave loss of the MZM structure in Fig.1, including electrode structure and semiconductor materials induced loss, with varying p-cladding layer doping concentration using HFSS. Fig. 3 shows that for a 1.7 μm thickness p-cladding layer MZM design, temperately increasing p-cladding layer doping concentration from 1×10^{17} cm^{-3} to 1×10^{18} cm^{-3} can reduce R_p without stimulating greater R_{sc}, leading to improved microwave attenuation at 60 GHz from 7.1 dB/mm to 2.9 dB/mm, which will significantly affect the mm scale TWE MZM modulation bandwidth at high frequency. Moreover, further improved microwave loss can be achieved when we decrease the p-cladding layer thickness from 1.7 μm to 1.3 μm and this is mainly caused by distinctly reduced R_p. Our simulation results in Fig. 3 demonstrate that the p-cladding layer conductivity shows opposite effects in light and heavy doping regimes for a TWE-MZM. In a light doping regime, the shunt current within the p-cladding layer induced transverse semiconductor loss dominants the microwave attenuation factors. In a heavy doping regime, the longitudinal current induced longitudinal semiconductor loss appears to take the leading role.

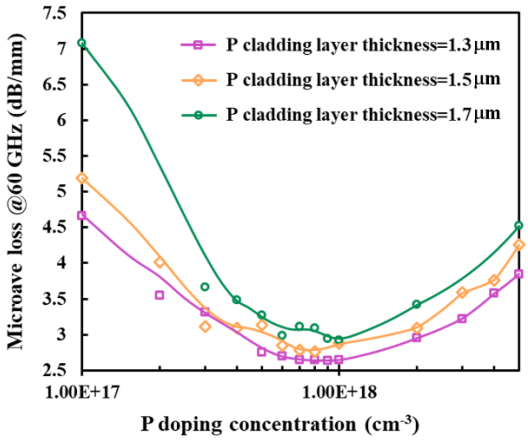

Fig. 3. Simulated microwave loss at 60 GHz for varying p-type doping concentrations of the p-cladding layer.

Fig. 4 shows the simulated electro-optic (EO) response of a 2 mm TWE length InP MZM design with 1.3 μm thickness p-cladding layer of 1×10^{17} cm^{-3}, 3×10^{17} cm^{-3}, 5×10^{17} cm^{-3} and 1×10^{18} cm^{-3} doping concentrations, the 3-dB bandwidths are 48 GHz, 61 GHz, 65 GHz and 67 GHz respectively. It should be noted that increasing p-type dopant will cause extra optical free-carrier absorption loss due to its overlap with the optical mode in the MQW region, which can be simulated from Lumerical. To tradeoff between microwave and optical loss due to p-type dopant, we select 5×10^{17} cm^{-3} as the optimal doping concentration for the proposed MZM design (Fig. 1), corresponding to 65 GHz 3-dB bandwidth and 0.36 dB/cm free-carrier absorption loss.

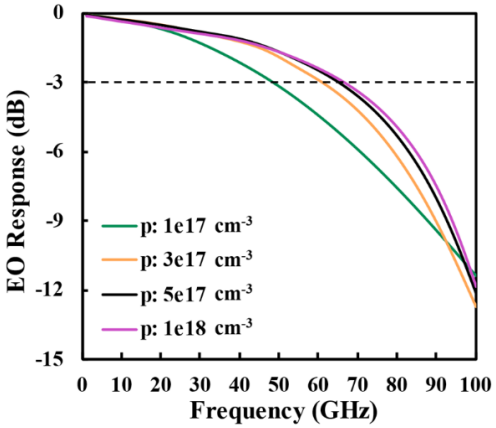

Fig. 4. Simulated EO response of a 2 mm TWE length InP MZM design with 1.3 μm thickness p-cladding layer of multiple doping concentrations.

IV. Conclusion

In conclusion, we present in-depth analysis on multiple microwave loss mechanisms in the total attenuation of TWE-MZM, including the p-cladding layer induced transverse and longitudinal semiconductor losses by full-wave simulation. In contrast with previously published lossless transmission line treatment [4], [5], the present full-wave analysis takes semiconductor losses within p-cladding layer into consideration. This is important since the p-cladding layer induced transverse and longitudinal semiconductor losses are found to significantly influence the MZM 3-dB bandwidth. Accordingly, the earlier lossless transmission line model is deemed inadequate for accurate analysis of these TWE-MZM. Our analysis provides possibilities for breaking InP MZM high-speed performance bottleneck to 200 Gb/s by minimizing semiconductor microwave propagation attenuation on a general p-i-n type platform, which is easy to fabricate and exhibits relatively low cost in high volume commercial applications.

References

[1] S. Arafin and L. A. Coldren, "Advanced InP Photonic Integrated Circuits for Communication and Sensing," in IEEE Journal of Selected Topics in Quantum Electronics, vol. 24, no. 1, pp. 1-12, Jan.-Feb. 2018, Art no. 6100612, doi: 10.1109/JSTQE.2017.2754583.

[2] R. G. Walker, "High-speed III-V semiconductor intensity modulators," in IEEE Journal of Quantum Electronics, vol. 27, no. 3, pp. 654-667, March 1991, doi: 10.1109/3.81374.

[3] R. Lewen, S. Irmscher and U. Eriksson, "Microwave CAD circuit modeling of a traveling-wave electroabsorption modulator," in IEEE Transactions on Microwave Theory and Techniques, vol. 51, no. 4, pp. 1117-1128, April 2003, doi: 10.1109/TMTT.2003.809669.

[4] G. L. Li, T. G. B. Mason and P. K. L. Yu, "Analysis of segmented traveling-wave optical modulators," in Journal of Lightwave Technology, vol. 22, no. 7, pp. 1789-1796, July 2004, doi: 10.1109/JLT.2004.831179.

[5] M. Stepanenko, I. Yunusov, V. Arykov, P. Troyan, and Y. Zhidik, “Multi-Parameter Optimization of an InP Electro-Optic Modulator,” Symmetry, vol.12, no.11, p.1920, Nov.2020, doi: 10.3390/sym12111920.

[6] Y. Ogiso et al., "80-GHz Bandwidth and 1.5-V Vπ InP-Based IQ Modulator," in Journal of Lightwave Technology, vol. 38, no. 2, pp. 249-255, 15 Jan.15, 2020, doi: 10.1109/JLT.2019.2924671.

[7] Inspec (Ed.). "Properties of Indium Phosphide." Inspec (1990).

[8] Kwon, Y. R., Hietala, V. M., and Champlin, K. S., “Quasi-TEM analysis of 'slow-wave' mode propagation on coplanar microstructure MIS transmission lines”, IEEE Transactions on Microwave Theory Techniques, vol. 35, pp. 545–551, 1987. doi:10.1109/TMTT.1987.1133702.